Journal of Environmental Management 380 (2025) 125130

Contents lists available at ScienceDirect

Journal of Environmental Management

journal homepage: www.elsevier.com/locate/jenvman

Research article

Sustainable, highly effective selenate removal using electrochlorination facility–obtained magnesium precipitate: An approach to in situ layered double hydroxide formation

Han Gyeol Jeon [a], Jin-Seok Kim [b], Seonggyu Choi [b,d], Kyung-Hee Lee [c], Kyoung-Woong Kim [a,*], Sang-Ho Lee [b,e,**]

[a] Department of Environment and Energy Engineering, Gwangju Institute of Science and Technology (GIST), Gwangju, 61005, Republic of Korea
[b] Disposal Performance Demonstration R&D Division, Korea Atomic Energy Research Institute, Daejeon, 34057, Republic of Korea
[c] Central Research Institute, Korea Hydro & Nuclear Power (KHNP), Daejeon, 34101, Republic of Korea
[d] Department of Radiochemistry, University of Science and Technology, Daejeon 34113, Republic of Korea
[e] Department of Nuclear Science and Technology, University of Science and Technology, Daejeon 34113, Republic of Korea

ARTICLE INFO

Keywords:
Magnesium precipitate
Selenate
Layer double hydroxide
Surface complexation
Adsorption

ABSTRACT

We proposed a sustainable selenate (Se(VI)) removal method using in situ layered double hydroxide (LDH) formation and calcined magnesium precipitate (CMP) derived from an electrochlorination facility. During kinetic experiments, the optimal removal conditions were identified by adjusting pH and Al dosage, which enabled a notable Se(VI) removal efficiency (127 mg/g-CMP). The initial release of Mg ions from CMP was confirmed to occur via Al-ion hydrolysis. Subsequently, after the pH adjustment process, Se(VI) could be sequestered via outer-sphere complexation within the interlayer space of the brucite-like sheets in LDH. The reusability of precipitated sludges (LDHS and calcined LDHS (LDOS)), which can be secondary wastes, was also evaluated as Se(VI) adsorbents. The results confirmed the high maximum adsorption capacity of LDOS (42.1 mg/g), demonstrating its performance comparable to that of reported adsorbents. This study highlights the potential of the in situ LDH formation method for Se(VI) removal and the possibility of transforming magnesium precipitate into sustainable resources.

1. Introduction

Se is a metalloid and trace element that is naturally released into the environment by the weathering of the earth's crust (Su and Suarez, 2021). It can be further discharged into aquatic ecosystems by anthropogenic activities, such as mining, agriculture, and oil refining (Ullah et al., 2019, 2023). Although it is an essential element for humans, excessive exposure to Se can cause hair loss, cytotoxicity, and DNA damage (Letavayová et al., 2006; Ruj et al., 2022; Shao and Zheng, 2008). Se is present in various chemical states (selenide, Se(−II); elemental Se, Se(0); selenite, Se(IV); and selenate, Se(VI) (Liang et al., 2013)). In neutral pH and oxidized conditions, it mainly exists as trigonal pyramidal Se(IV) and tetrahedral Se(VI) oxyanions (Sharmasarkar and Vance, 2002). However, both oxidized species (Se(IV) and Se(VI)) possess higher toxicities than the reduced species (Se(−II) and Se(0)) (Ullah et al., 2019). The occurrence of ^{79}Se, a fission product with a very long half-life (~1.13×10^6 years (Frechou et al., 2007)), has also increased the necessity for Se remediation. Therefore, many researchers have explored diverse methods for removing Se(IV) and Se(VI), such as adsorption and coprecipitation (Guo et al., 2017;

Abbreviations: $AlCl_3$, aluminum chloride; C_0, initial concentration; CMP, calcined magnesium precipitate; CLDHS, recalcined layered double hydroxide sludge; CO_3^{2-}, carbonate; EC, electrical conductivity; EXAFS, extended X-ray absorption fine structure; F^-, fluoride; FE-SEM, field-emission scanning electron microscopy; FTIR, Fourier-transform infrared spectroscopy; HA, humic acid; HCl, hydrochloric acid; HNO_3, nitric acid; LDH, layered double hydroxide; LDHS, layered double hydroxide sludge; MP, magnesium precipitate; NaOH, sodium hydroxide; Na_2SeO_4, sodium selenate; CO_2, carbon dioxide; NaCl, sodium chloride; NaClO, sodium hypochlorite; NO_3^-, nitrate; NOM, natural organic matter; OH^-, hydroxide; PO_4^{3-}, phosphate; Se(IV), selenite; Se(VI), selenate; SEM, scanning electron microscopy; SO_4^{2-}, sulfate; USEPA, United States Environmental Protection Agency; XPS, X-ray photoelectron spectroscopy; XRD, X-ray diffraction; XRF, X-ray fluorescence.

* Corresponding author.
** Corresponding author.
E-mail addresses: kwkim@gist.ac.kr (K.-W. Kim), sangholee@kaeri.re.kr (S.-H. Lee).

https://doi.org/10.1016/j.jenvman.2025.125130
Received 28 November 2024; Received in revised form 9 March 2025; Accepted 22 March 2025
Available online 29 March 2025

Jordan et al., 2018; Lounsbury et al., 2016). Furthermore, recent research has focused on utilizing industrial and municipal waste materials for sustainable Se removal (Sun et al., 2017; Zoroufchi et al., 2023).

In power plants, electrochlorination facilities are generally installed to produce a large-scale sodium hypochlorite (NaClO) solution using seawater, which is then transferred to a storage tank. This solution is subsequently used to remove microorganisms that could negatively affect coolant systems in turbines (Lee et al., 2020). However, owing to the high pH condition of the NaClO solution and the presence of Mg ions in seawater, magnesium precipitate (MP) accumulates as low-crystalline brucite ($Mg(OH)_2$) at the bottom of the storage tank (Lee et al., 2020). Although the brucite in MP can be readily transformed into magnesium oxide (MgO) by calcination (CMP) and MgO is particularly effective at sequestering anionic pollutants (Chinthala et al., 2021; Duan et al., 2022), MP is being discarded as waste near the power plant. Hence, in our previous study, MP was simply calcined to produce a sustainable MgO-based adsorbent (CMP) aimed at Se(IV) and Se(VI) sequestration (Jeon et al., 2024). CMP exhibited high Se(IV) removal efficiency, whereas Se(VI) showed a low affinity. This difference could be attributed to their different adsorption mechanisms—inner-sphere predominant surface complexation for Se(IV) and outer-sphere complexation for Se(VI) onto CMP, based on MgO. Consistent with these findings, Se(IV) generally tends to form strong complexes on the surfaces of soil minerals in nature, while Se(VI) is more readily leached (Goh and Lim, 2004; Peak, 2006; Zelmanov and Semiat, 2013). The difference in adsorption affinities between Se(IV) and Se(VI) has also been observed with other oxide-based adsorbents (Table 1). In addition, Guo et al. (2017) reported a different Se(IV) and Se(VI) removal trend (i.e., low Se(VI) removal efficiency) when employing the ettringite coprecipitation. Therefore, it is crucial to examine and select an appropriate method for the effective Se(VI) sequestration in aqueous phases.

Layered double hydroxides (LDHs, $[M^{2+}_{1-x}M^{3+}_{x}(OH)_2]^{x+}(A^{n-})_{x/n}\cdot mH_2O$) are clay minerals exhibiting brucite-like layered structures. The divalent (M^{2+}: Mg^{2+}, Fe^{2+}, and Ca^{2+}) and trivalent (M^{3+}: Al^{3+}, Fe^{3+}, and Cr^{3+}) cations in each LDH sheet comprise a positively charged layer. The charge of each layer is balanced by anion (A^{n-}: OH^-, Cl^-, NO_3^-, CO_3^{2-}, etc.) intercalation to form the layered structure (Theiss et al., 2016). Generally, the interlayer of LDH exhibits weak bonding, allowing the substitution of interlayer ions with other anionic substances in aqueous solutions (Cavani et al., 1991; Goh et al., 2008). Thus, LDH has been employed as a host for anionic pollutants, such as As, Sb, P, and Cr (Das et al., 2006; Goswamee et al., 1998; Lee et al., 2018b; Lee and Takahashi, 2019). In line with this, Chubar and Szlachta (2015) investigated Se(VI) removal using CO_3-intercalated Mg/Al LDH and reported Se(VI) removal capacities of 103 and 45.6 mg/g at pH 5.0 and 7.5, respectively. These capacities were higher than those of reported metal oxide-based adsorbents (Table 1), demonstrating the suitability of LDH for Se(VI) sequestration, which is challenging to achieve.

Various LDH synthesis methods have been studied, including coprecipitation, hydrothermal, and urea hydrolysis (Jing et al., 2010; Theiss et al., 2016). Among these methods, coprecipitation is regarded as the most economically effective (Cavani et al., 1991). To further reduce the synthesis cost and address environmental concerns, abundant and sustainable solid precursors from natural ores and industrial wastes have been considered for LDH synthesis (Devi and Saroha, 2017; Jiang et al., 2023; Kuwahara and Yamashita, 2013; Muriithi et al., 2017; Qiu et al., 2013; Rybka et al., 2022). In this respect, the efficient extraction of metal ions is key to producing solid-precursor-based LDHs (Jiang et al., 2023; Muriithi et al., 2017). However, the extraction process often requires strong acids, such as hydrochloric acid (HCl) and nitric acid (HNO_3), which are not eco-friendly (Muriithi et al., 2017). To overcome this hurdle, Rybka et al. (2022) recently explored applying magnesite in Mg/Al LDH synthesis via Al hydrolysis, which can generate hydronium ions (H_3O^+) to ionize the solid precursors directly (Fig. S1). Their study found that the removal efficiency of magnesite-based Mg/Al LDH for anionic pollutants was comparable to that of conventionally synthesized LDHs.

After extracting metal ions (e.g., Mg^{2+}) from the solid precursor via Al hydrolysis, a positively charged sheet can form under alkaline conditions. Subsequently, instead of generally hosted ions (e.g. Cl^-, NO_3^-, CO_3^{2-}, etc.), anion pollutants, such as As and Cr, can be directly intercalated in the interlayer and then coprecipitated as the LDH phase (Chao et al., 2018; Wang et al., 2021). This in situ LDH formation method can streamline the operational steps (Figs. S1 and S2) required to sequester anionic pollutants compared to pre-synthesized LDH adsorbents, offering greater convenience (Chao et al., 2018; Huang et al., 2019; Wang et al., 2021). However, this method has rarely been explored for Se(VI) removal. To the best of our knowledge, solid waste precursors have not been utilized for the in situ LDH formation method so far. Furthermore, the reusability of the precipitated sludge has not been extensively

Table 1
Se removal capacities of various adsorbents compared to the in-situ LDH formation method using CMP.

Adsorbents	Initial pH	q_m (mg/g)		Ref.
		Se(IV)	Se(VI)	
Water treatment sludge	5	21.1	11.1	Zhou and Haynes (2012)
Nano TiO_2	5.8	3.40	2.73	Yamani et al. (2014)
Nano Al_2O_3	5.8	10.9	9.35	Yamani et al. (2014)
$MnFe_2O_4$	4	6.57	0.77	Gonzalez et al. (2010)
$CuFe_2O_4$	7.4	14.1	5.55	Sun et al. (2015)
α-Fe_2O_3	6.5	17.9	7.47	Lounsbury et al. (2016)
α-FeOOH	3	13.7	6.30	Yue et al. (2020)
ZVI supported bentonite-zeolite	4		1.44	Phanthasri et al. (2023)
Fe/Si coprecipitates	5	22.5	15.2	Chan et al. (2018)
LDH-coated zerovalent iron	–		35.0	Xu and Huang (2019)
Iron-loaded food-waste biochar	7		11.7	Hong et al. (2020)
Fe/cattle manure-biochar	7		52.6	Lee et al. (2021)
Sulfur loaded magnetic microsphere	6	25.8	9.25	Zhao et al. (2023)
Iron(III)-alginate with layered aluminum oxyhydroxide	6	11.1	10.0	Ren et al. (2024)
MgO nanosheets	10.5	103	10.3	Cui et al. (2018)
Mg/Al–CO_3 LDH	7	119	45.6	Chubar and Szlachta (2015)
Magnesite based Mg/Fe LDH	5		19.7	Rybka et al. (2022)
$MgFeSO_4$-type LDH	9.5		78.7	Paikaray et al. (2013)
Calcined Mg/Al LDH	10		76.6	Tian et al. (2020)
Calcined magnesium precipitate	7	85.0	2.97	Jeon et al. (2024)
In situ LDH formation using CMP	**7**		**127**	**This study**
LDHS	**7**		**12.8**	**This study**
LDOS	**7**		**42.1**	**This study**

demonstrated, although the sludge becomes a secondary waste. Therefore, this study aimed to (1) apply CMP as a solid precursor and Mg source for Se(VI) removal via in situ LDH formation; (2) investigate the effect of pH, Al concentrations, CMP dosage, and co-existing ions to determine optimal operation conditions; (3) verify the sequestration pathway of Se(VI) using this novel approach; and (4) assess the reusability of the precipitated sludge as a Se(VI) adsorbent for sustainability.

2. Materials and methods

2.1. Materials

All chemicals in this study were obtained from Sigma-Aldrich. Sodium selenate (Na_2SeO_4, ≥99%) and aluminum chloride ($AlCl_3$, ≥99%) hexahydrate were used to prepare 1000 mg/L Se(VI) and 0.5 M Al stock solutions. The solution pH was adjusted with 0.5 M NaOH and 0.5 M HCl. The MP was sampled during the cleaning of a hypochlorous-acid storage tank near a power plant in South Korea. The MP was rinsed with DI water until solution conductivity was <100 μS/cm, fully dried at 60 °C, and ground to pass a 100-mesh (150 μm) sieve. The prepared MP was calcined (CMP) for 2 h at 500 °C with a heating rate of 3 °C min^{-1} and stored at a dry keeper to prevent moisture absorption.

2.2. Removal of selenate via in situ LDH formation and the generated sludge

Kinetic experiments were conducted to investigate the effect of pH and the Al concentration on Se(VI) removal via in situ LDH formation. The influence of CMP dosage and co-existing anions on the removal process was verified while maintaining a Mg to Al molar ratio (5:1) with a pH adjustment to 10. The Se(VI) adsorption experiments were performed using the generated sludge as a result of the removal process. Detailed experimental procedures for Se(VI) removal and adsorption experiments are provided in the Supplementary Material and Fig. S2.

2.3. Characterization

The oxide compositions of CMP were initially determined by X-ray fluorescence (XRF; ARL PERFORM'X, Thermo Fisher Scientific, USA). The particle size distribution and zeta potential of the sample were assessed using a particle size analyzer (Mastersizer 3000, Malvern Panalytical, UK) and a zeta potential analyzer (Zetasizer Nano ZSP, Malvern Panalytical, UK), respectively. The surface morphology was examined by field-emission scanning electron microscopy (FE-SEM; SU8600, Hitachi, Japan) with energy-dispersive spectroscopy (EDS). Crystal phases were analyzed by X-ray diffraction (XRD; SmartLab, Rigaku, Japan) with Cu Kα 1 radiation (λ = 1.5406 Å). XRD patterns of samples were measured at a scanning speed of 2° min^{-1} with a scanning step of 0.01° over the 5°–70° range and quantitative fractions of the crystal phases were calculated using Rietveld refinement (Mccusker et al., 1999; Rodríguez-Carvajal, 2021). Crystallite sizes were determined using Scherrer's equation (Cullity, 1956). Crystal phases of MP and CMP were analyzed by XRD, and the result is shown in Fig. S3a. Vibrational modes of the samples were examined by Fourier-transform infrared spectroscopy (FTIR; Vertex 70v, Bruker, USA). Further, X-ray photoelectron spectroscopy (XPS; NEXSA, Thermo Fisher Scientific, USA) with a monochromated Al Kα X-ray source was used to analyze chemical states on the sample surfaces. Survey and narrow XPS spectra were obtained with step sizes of 1 eV and 0.1 eV, respectively.

3. Results and discussion

3.1. Effects of pH

Fig. 1a–d shows changes in the Se(VI) fraction, Mg and Al concentrations, and pH over time during the reaction. The initial pH of all Se

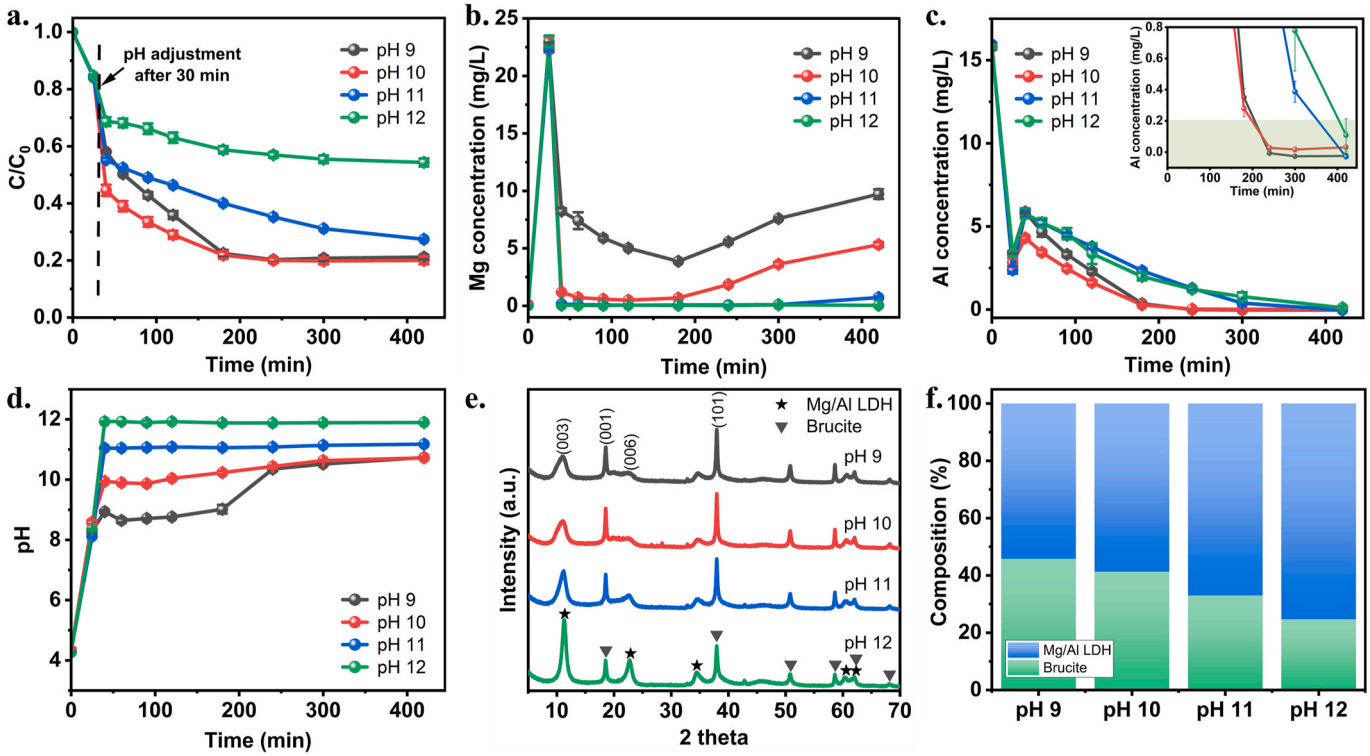

Fig. 1. Effects of the pH values on the dissolved fractions of (a) Se(VI), (b) Mg, and (c) Al and (d) pH over time during in situ LDH formation (initial Se(VI) concentration (C_0): 20 mg/L, CMP dosage: 0.133 g/L (corresponding to 3 mM MgO in CMP), Al dosage: 0.6 mM, pH adjustment range: 9–12, and temperature: 20–23 °C). (e) XRD patterns, including brucite (PDF No. 96-100-0055) and Mg/Al LDH (hydrotalcite) (PDF No. 96-900-9273), and (f) crystal-phase compositions (determined by Rietveld refinement) of the in situ–formed LDH sludges.

(VI)-containing solutions was set to 7. However, following the addition of 0.6 mM Al before adding CMP, the pH values of all solutions decreased to 4.2. It could be due to H_3O^+ ions produced by Al hydrolysis with water molecules (Eq. (1)) (Schofield and Taylor, 1954). After 20 min of adding CMP, we observed an increase in the Mg concentration, attributed to the partial dissolution of MgO in CMP (Eqs. (2) and (3)) (Fruhwirth et al., 1985)). Consequently, the pH values of all solutions might have increased to 8.1–8.3 (Fig. 1d). However, the formation of the Mg/Al LDH phase is challenging at these pH conditions (Chen et al., 2021; Wu et al., 2018); therefore, we inferred that Se(VI) removal efficiency was low at this stage (Fig. 1a). Put differently, a sufficient basic condition was required for the nucleation and formation of the Mg/Al LDH phase, which acts as a host for Se(VI). Thus, the pH values of all solutions were adjusted to 9–12 using 0.5 M NaOH after 30 min of CMP addition. Next, XRD analysis was performed to determine the crystal phases of each generated sludge after the reaction (Fig. 1e). Diffraction peaks corresponding to the (003) and (006) planes of Mg/Al LDH and (101) plane of brucite ($Mg(OH)_2$) were observed in the patterns. The presence of two different phases might be attributable to the partial dissolution of the MgO from CMP into Mg ions (Fig. 1b), facilitating the formation of the LDH phase, and the hydration of the residual MgO into the brucite phase. For the quantitative analysis of each crystal phase, Rietveld refinement was performed (Fig. 1f). The results indicated that the weight fraction of the LDH phase increased from 54.2% to 75.3% with elevating pH. The crystallite size of each LDH phase also increased from 47.3 to 98.9 Å as the pH of adjusted solutions was elevated (Table 2).

$$Al^{3+} + H_2O \rightarrow AlOH^{2+} + H^+ \quad (1)$$

$$MgO + 2H^+ \rightarrow Mg^{2+} + H_2O \quad (2)$$

$$MgO + H_2O \rightarrow Mg^{2+} + 2OH^- \quad (3)$$

The XRD results suggest that the LDH formed by pH adjustment significantly enhanced Se(VI) removal (Fig. 1a). However, the lowest removal efficiency was observed when the pH was adjusted to 12, despite even the highest weight fraction of LDH in the sludge (72.9%). Generally, an increase in the crystallite size causes a reduction in the surface area of an adsorbent, lowering its sorption affinity for an adsorbate (Ivanets et al., 2021; Wang et al., 2013). In addition, previous studies have reported that the point of zero charge (pH_{pzc}) of Mg/Al LDH is approximately 10–12 (Goh et al., 2008; Han et al., 1998; Jiang et al., 2021), which aligned with our zeta potential results for in situ formed LDH sludge in Fig. S4. As a result, the pH elevation rendered the Mg/Al LDH surface more negatively charged, thereby increasing its electrostatic repulsion against anionic substances. (Gu et al., 2016). The presence of more hydroxide ions (OH^-) could also contribute to competition with Se(VI) (Sato et al., 1992; Theiss et al., 2014), which may lead to a lower removal efficiency. Conversely, the highest efficiency was observed by adjusting the pH to 10 compared with the pH adjustment to 12 (Fig. S5a). Additionally, the sludge obtained at pH 10 (50.7 Å) exhibited a larger crystallite size than that obtained at pH 9 (47.3 Å), while the removal efficiencies at pH 9 were relatively similar (Table 2 and Fig. S5a). The crystallite size represents a crucial factor in the removal process by in situ LDH formation, as a smaller crystallite size can inhibit the sedimentation of the generated sludge (Tsuchiya et al., 2023). In addition, the variation in crystallite size showed a similar trend to the size of the sheet-like particles observed by SEM analysis (Fig. 3). Based on these findings, adjusting the pH value to 10 for LDH formation appeared to be optimal for Se(VI) removal. Hence, this optimal pH was applied in the subsequent experiments.

Concurrently, as shown in Table S1 and presented in Fig. S7, XRF analysis of CMP revealed that the Ca content (as CaO, 3.65%) was very low compared with the Mg content (as MgO, 91.15%) and the concentration of Ca (Fig. S7) did not change significantly compared with that of Mg (Fig. 1b) during the reaction. Furthermore, a possible Ca-related mineral phase for Se(VI) sequestration, such as hydrocalumite (Ca/Al LDH) or $CaSeO_4$, was not detected by the XRD analysis. These findings indicated that the influence of Ca could be excluded under the optimal condition.

Table 2
Effect of Al dosage and pH on the crystallite sizes of the in situ–formed sludge.

pH	Al concentration (mM)	Mg/Al (molar ratio)	Crystallite size (Å)[a]
9	0.6	5	47.3
10	0.6	5	50.7
11	0.6	5	72.1
12	0.6	5	98.9
10	0.3	10	53.3
10	1	3	52.0
10	3	2	51.4

[a] Mean crystallite size determined by the full width at half maximum of (0 0 3) and (0 0 6) peaks using Scherer's equation.

3.2. Effect of the aluminum dosage

The molar ratio of M^{2+}/M^{3+} (Mg^{2+}/Al^{3+}) in LDH can significantly influence its anionic-pollutant-scavenging ability (Huang et al., 2019; Wang et al., 2021; You et al., 2001). Therefore, we evaluated the effect of Al concentration on Se(VI) removal and measured changes in Mg and Al concentrations and solution pH during the experiment (Fig. 2a–d). Upon adding different Al concentrations to Se(VI)-containing solutions, a further pH decrease was observed, particularly at higher Al concentrations (Fig. 2d). This decrease was attributed to the increased concentration of Al ions, thereby facilitating hydrogen ions generation, as indicated in Eq. (1). Consequently, more MgO in CMP dissolved into Mg ions in the stronger acidic environment at 20 min after CMP addition (Fig. 2b). Contrary to the result described in Fig. 1a (Section 3.1.), lower Se(VI) fractions were observed at 1 and 1.5 mM Al concentrations at this reaction time (Fig. 2a). Considering the acidic pH of 4.5–5.5 at this reaction time (20 min after adding CMP, Fig. 2d), LDH phase generation is challenging. Under similar pH conditions to our results, previous studies have reported that Al ions preferentially precipitate as $Al(OH)_3$ (Eqs. (4) and (5)), whereas Mg ions remain in a dissolved form, (Boclair and Braterman, 1999; Saha et al., 2017; Tsuchiya et al., 2023). Thus, the precipitation of Al ions might be attributed to the significant decrease in Al concentration observed at 20 min of reaction time (Fig. 2c). Additionally, aluminum hydroxide ($Al(OH)_3$), the precipitated form of Al (e.g., gibbsite), is known to exhibit affinity toward Se(VI), and this may account for the lower fraction of Se(VI) observed in our study (Xi et al., 2023). However, under our experimental conditions, the solutions mixed with CMP without pH adjustment remained unseparated into distinct liquid and solid phases, even after prolonged sedimentation (Fig. S8). This indicated that pH adjustment is necessary to achieve effective separation and ensure practical operation.

$$xAl^{3+} + 3xOH^- \rightarrow xAl(OH)_3(s) \quad (4)$$

$$xAl(OH)_3(s) + xOH^- \rightarrow x[Al(OH)_4]^- \quad (5)$$

$$(1-x)Mg^{2+} + x[Al(OH)_4]^- + (2-4x)OH^- \rightarrow \left[Mg_{1-x}{}^{2+}Al_x{}^{3+}(OH)_2\right]^{x+} \quad (6)$$

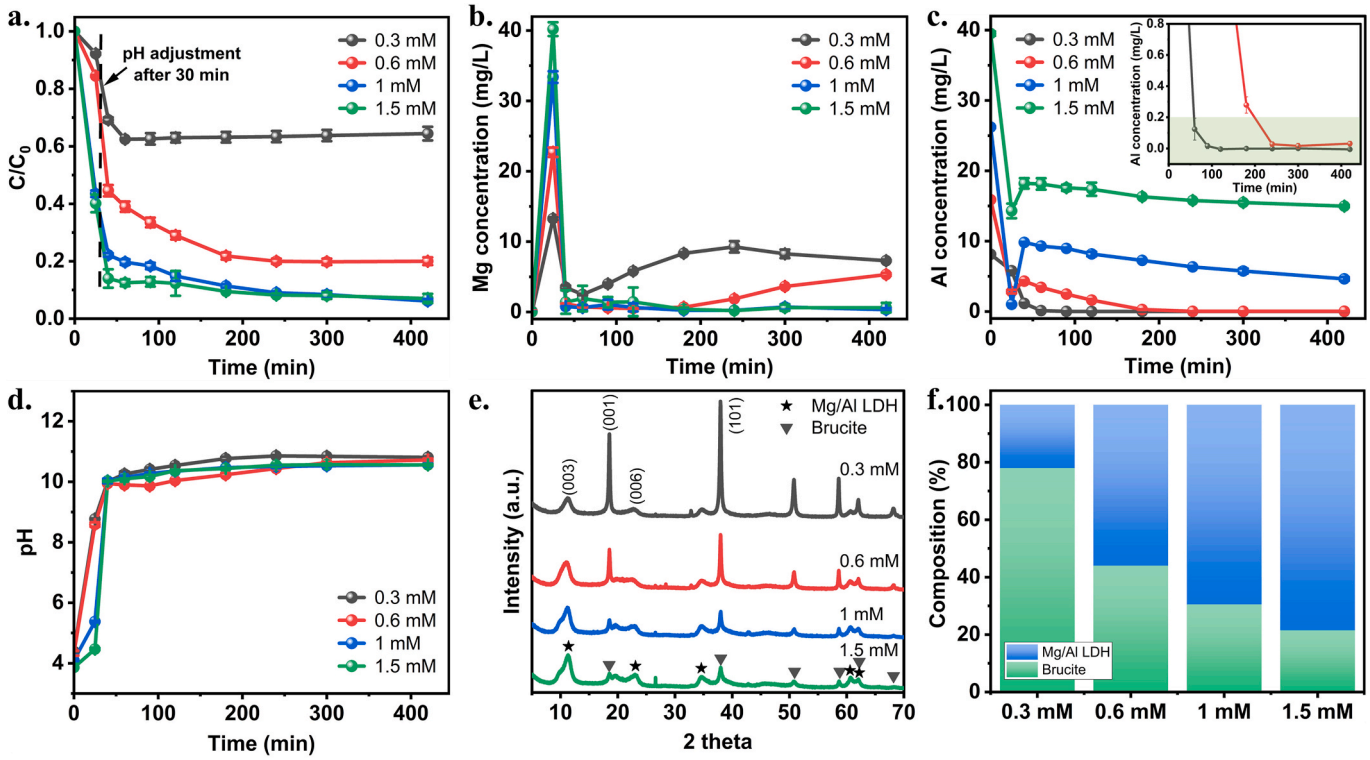

Fig. 2. Effects of the Al dosages (0.6–1.5 mM) on the dissolved fractions of (a) Se(VI), (b) Mg, and (c) Al and the (d) pH over time during in situ LDH formation (C_0: 20 mg/L, CMP dosage: 0.133 g/L (corresponding to 3 mM MgO in CMP), pH adjustment: 10, and temperature: 20–23 °C). (e) XRD patterns, including brucite (PDF No. 96-100-0055) and Mg/Al LDH (hydrotalcite) (PDF No. 96-900-9273), and (f) crystal-phase compositions (determined by Rietveld refinement) of the in sit-u–formed LDH sludges.

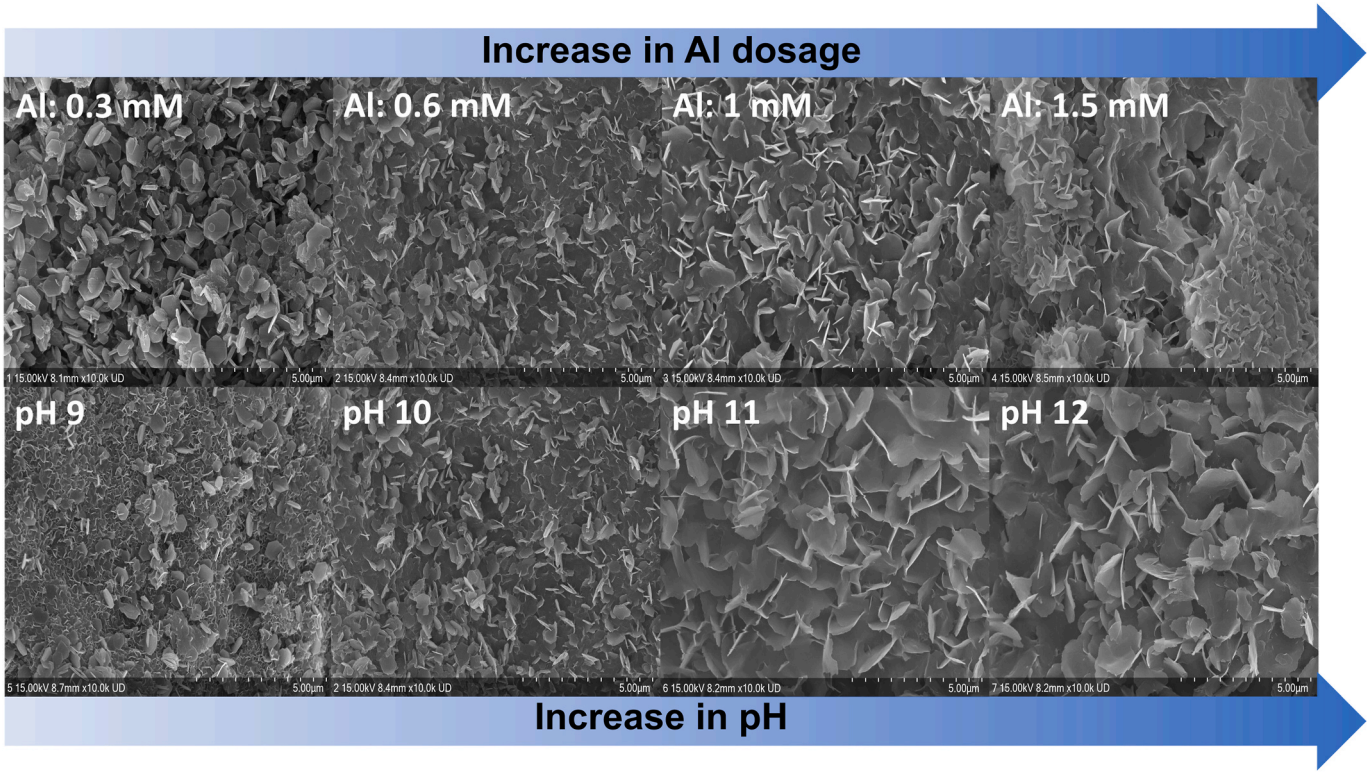

Fig. 3. SEM images of the in situ–formed LDH sludges during Se(IV) removal at varying pH values (9–12 with 0.6 mM Al) and Al dosages (0.6–1.5 mM with a pH adjustment to 10).

$$\left[Mg_{1-x}{}^{2+}Al_x{}^{3+}(OH)_2\right]^{x+} + (A^{n-})_{x/n} \rightarrow \left[Mg_{1-x}{}^{2+}Al_x{}^{3+}(OH)_2\right]^{x+}(A^{n-})_{x/n} \bullet mH_2O \quad (7)$$

After adjusting the pH values of all solutions to 10 and completing the reaction, XRD analyses of the generated sludges were performed (Fig. 2e). The peak intensities of the (003) plane of the LDH phase increased, while those of the (001) plane of the brucite phase decreased with the increasing Al concentration, indicating that the weight fraction of LDH phases increased with the higher Al concentration (Fig. 2f). This result might correspond to the greater thermodynamic stability of LDH compared with that of brucite (Bernard et al., 2022). Put differently, the higher Al ion concentration enhanced MgO dissolution into Mg ions through Al hydrolysis (Fig. 2b). The dissolved Mg ions then preferentially contributed to LDH formation by pH adjustment, as described in Eqs. (6) and (7), A^{n-} represents SeO_4^{2-} and Cl^-, and $0.2 < x < 0.33$) (Forano et al., 2006; Min et al., 2022; Saha et al., 2017; Zhu et al., 2021), rather than reprecipitating into brucite owing to differences in thermodynamic stability. The more reduced Se(VI) fraction at higher Al concentrations (1 and 1.5 mM) might be ascribed to the increased LDH phase quantity at the same pH conditions (Fig. 2a). Meanwhile, the United States Environmental Protection Agency (USEPA) regulates maximum Al concentration to 0.2 mg/L (USEPA, 2017) due to its toxicity. However, the residual Al concentrations at higher Al dosages (1 and 1.5 mM) were 4.6 and 15.0 mg/L, respectively, whereas the concentrations were below the standard at 0.3 and 0.6 mM (Fig. 2c). Hence, the optimal Al dosage was determined to be 0.6 mM, equivalent to a Mg/Al molar ratio of 5. Under these optimal conditions (Mg/Al ratio of 5 and pH 10), the Se(VI) removal capacity per CMP amount reached 127 mg/g-CMP (Fig. S5), which was significantly higher than the reported efficiencies with various adsorbents (Table 1). This highlighted the superior Se(VI) removal ability of this method.

3.3. Effect of CMP dosage

To achieve a maximum Se(VI) removal efficiency, CMP dosage was varied under the obtained optimal Mg/Al molar ratio of 5 and pH adjustment to 10 (Fig. 4d). The initial Se(VI) concentration was set at 20 mg/L, which is the highest reported Se(VI) concentration discharged from industrial effluents (Santos et al., 2015; Stefaniak et al., 2018). Se (VI) removal efficiency increased with a greater MgO content (higher CMP dosage) and nearly reached the maximum at a MgO molarity of 6 mM (corresponding to 0.265 g/L CMP). The highest Se(VI) removal efficiency was achieved at a 12 mM MgO dosage (0.531 g/L CMP), resulting in a residual Se(VI) concentration of 0.24 mg/L, with a removal efficiency of 98.8%. Although this concentration did not meet the USEPA standard, 0.05 mg/L (USEPA, 2024), the result demonstrates the significant potential of this in situ method to effectively reduce Se(VI) levels from a highly contaminated condition, i.e., 20 mg/L Se(VI). Moreover, the residual Al concentration remained below 0.05 mg/L in all solutions, indicating that no further Al treatment process was necessary.

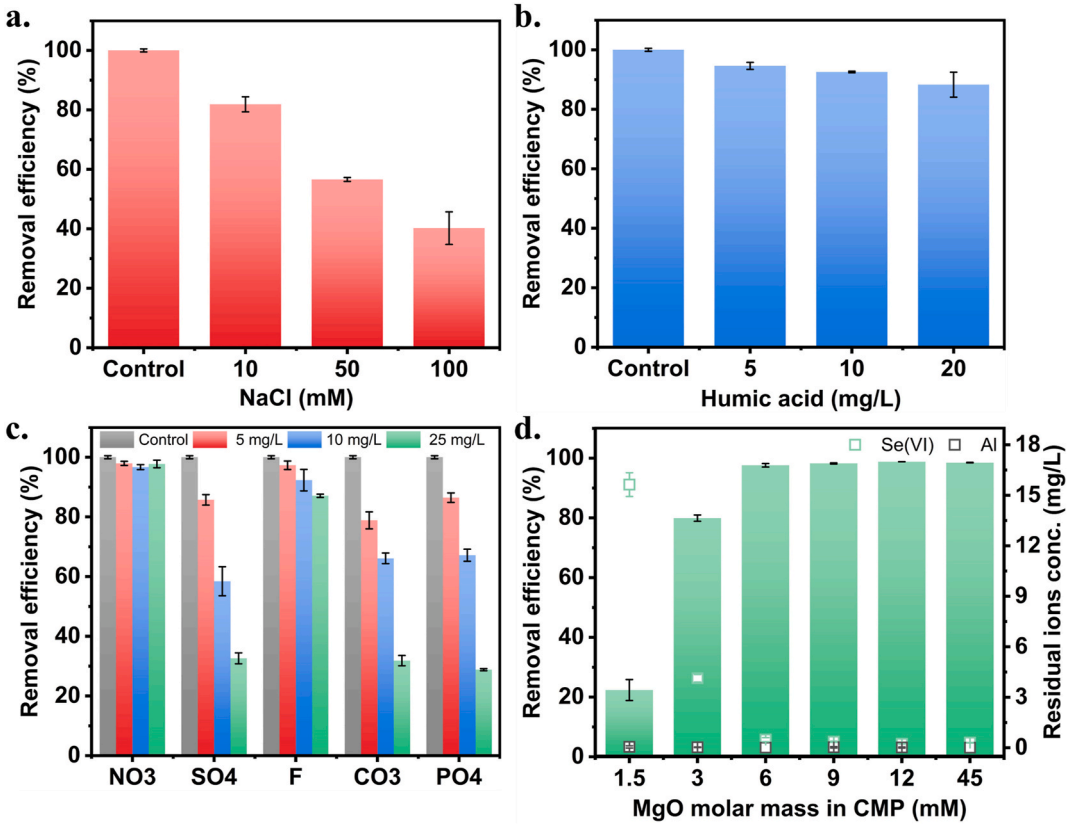

Fig. 4. Effects of the (a) ionic strength, (b) humic acid (HA), (c) co-existing anions, and (d) CMP dosage on the Se(VI) removal efficiency via in situ LDH formation (C_0: 10 mg/L for (a–c) and 20 mg/L for (d), CMP dosage: 0.133 g/L (except for (d)), Al dosage: 0.6 mM (except for (d)), pH adjustment: 10, temperature: 25 °C, and reaction time: 12 h).

3.4. Effects of the ionic strength and co-existing ions

The effect of the ionic strength and natural organic matter (NOM) on Se(VI) removal by this method was assessed at different concentrations of NaCl and humic acid (HA) (Fig. 4a and b). Results showed a remarkable decrease in Se(VI) removal efficiency with increasing NaCl concentration, likely due to weakened electrostatic attraction, a mechanism for separating charged pollutants (Gu et al., 2016). Additionally, outer-sphere complexation is generally sensitive to a change in the electrostatic attraction (Gu et al., 2016). HA, a typical NOM, can negatively affect removal efficiency by forming complexes on adsorptive surfaces, thereby impeding the removal process. Fig. 4b shows that the Se(VI) removal efficiency decreased by only ~11% in the presence of 20 mg/L HA, which is generally the highest concentration observed in natural environments (Basumallick and Santra, 2017).

The influence of co-existing anions, including NO_3^-, SO_4^{2-}, F^-, CO_3^{2-}, and PO_4^{3-}, was further investigated at varying concentrations (Fig. 4c). At low co-existing ion concentrations (5 mg/L), Se(VI) removal efficiency remained at ≥80% compared to the control group. NO_3^- had minimal impact on removal, while a 15% decrease was observed with F^- at the higher co-existing ion concentrations (25 mg/L). In contrast, the co-existence of SO_4^{2-}, CO_3^{2-}, and PO_4^{3-} exerted an adverse effect on Se(VI) removal at the same concentrations, with the competition order as follows: $NO_3^- < F^- < SO_4^{2-} \approx CO_3^{2-} \approx PO_4^{3-}$. The negligible influence of NO_3^- might be attributed to its low adsorptive characteristics onto Mg/Al LDH surfaces (Constantino et al., 2017). Conversely, a strong interaction has been reported for F^- sorption onto oxide surfaces, which could exert a different effect (Gao et al., 2014; Pokrovsky et al., 2005). The significant impact of SO_4^{2-}, CO_3^{2-}, and PO_4^{3-} was similar to those in previous LDH studies (Constantino et al., 2017; Goh and Lim, 2010; Lee et al., 2018b; You et al., 2001). This is likely attributable to the greater affinity for ions with higher charge numbers compared with monovalent ions in the LDH interlayer (Cavani et al., 1991; Constantino et al., 2017).

3.5. Selenate removal mechanism

For the effective application and further development of this method, an understanding of the Se(VI) sequestration pathway is important. Accordingly, the pathway was investigated using SEM-EDS, XRD, FTIR, XPS, and batch test results. First, SEM-EDS analysis confirmed the uniform distribution of Se(VI) on the surface of the precipitated sludge after the Se(VI) removal process (Fig. S9). Next, the XRD patterns of precipitated samples obtained in the presence (with) and absence (without) of Se(VI) were compared (Fig. 5a). Similar to the patterns observed in the presence of Se(VI), peaks corresponding to the (003) and (006) planes of the LDH phase were also observed in the absence of Se(VI). This might be attributed to OH^- generated by the pH adjustment and Cl^- from the $AlCl_3$ solution, which acts as hosted anions to form the LDH phase even in the absence of Se(VI). The measured basal spacings were 7.88 Å without Se(VI) and 8.06 Å with Se(VI), indicating a difference in the interlayer spacing due to the presence of different intercalated anions, particularly Cl^- (0.181 nm (Custelcean and Moyer, 2007),) and Se(VI) (0.249 nm (Constantino et al., 2017),) in this case.

The FTIR spectra of samples with and without Se(VI) exhibited characterized peaks (Fig. 5b), including a strong peak at 419 cm^{-1} (attributed to the metal–oxygen bond within the LDH lattice), a peak at 3699 cm^{-1} (vibrations from Mg–OH stretching attributed to brucite generated from hydrated CMP), a sharp band at 3453 cm^{-1} (associated with H-bonding from OH in the LDH interlayer LDH), and a peak at 1634 cm^{-1} (indicative of the physically adsorbed water molecules) (Chubar, 2014; Goh and Lim, 2010; Ji et al., 2017; Xu et al., 2020). The peak at 1372 cm^{-1} corresponds to CO_3^{2-} on the surface (Chubar, 2014; Palmer et al., 2009). likely sorbed during sample storage, as no CO_3^{2-}-containing chemicals were used in this study. The samples were also generated under closed experimental conditions to avoid the effect of CO_3^{2-}. Further, a peak at 876 cm^{-1} corresponding to Se(VI) was observed in the sample obtained in the presence of Se(VI) (Chubar, 2014; Su and Suarez, 2000). This result combined with the XRD findings indicated the intercalation of Se(VI) using this in situ method.

Fig. 5c–h shows the XPS full and narrow spectra and elemental compositions of samples with and without Se(VI). The Mg/Al ratios of the samples (4.8 and 4.47, respectively) were similar to the set molar ratio of 5 (Fig. 5c). In the absence of Se(VI), the Cl content was 1.24%; however, it decreased significantly in the presence of Se(VI), with a corresponding increase in the Se content. This indicated that divalent Se(VI) exhibited higher selectivity than monovalent Cl^- during the in situ LDH formation process involving Cl^- and Se(VI). Therefore, Se(VI) might preferentially intercalate into the LDH interlayer in the presence of Se(VI) and Cl^- ions, supporting the XRD result. Chubar (2014) investigated Se(VI) removal by Mg/Al LDH, demonstrating its superb sequestration. However, no chemisorption of Se(VI) with Mg or Al atoms was observed, indicating outer-sphere complexation due to long Mg/Al–Se(VI) distances observed by EXAFS analysis. Moreover, Se(VI) in the LDH phase was not reduced to Se(IV) in the sorption process. In another report, a significant decrease in the $Al(OH)_3$ peak was observed by XPS analysis when Se(VI) interacted with Mg/Al LDH (Chubar, 2018), indicating the primary localization of Se(VI) on the $Al(OH)_3$ surface regardless of chemisorption (outer-sphere complexation). In our high-resolution XPS results, no significant difference was observed in the Mg 2p spectra between samples (Fig. 5f), indicating that Mg atoms did not participate in Se(VI) sequestration. Meanwhile, the intensity of the $Al(OH)_3$ peak decreased in the deconvoluted Al 2p spectra (Fig. 5d), suggesting outer-sphere complexation driven by the primary localization of Se(VI) (Chubar, 2018). Consistent with the FTIR result in Fig. 5b, the Se(VI) peak in the Se 3d narrow spectra matched the Na_2SeO_4 reference (Fig. 5g), indicating no reduction occurred, as reported in previous studies (Chubar, 2014). Additionally, as discussed in Section 3.4., Se(VI) removal efficiency decreased with increasing ionic strength, a phenomenon that could be related to outer-sphere complexation (Gu et al., 2016). In summary, our results indicated that CMP preferentially dissolved via Al-ion hydrolysis upon the $AlCl_3$ addition, releasing Mg ions. Subsequently, pH adjustment to an alkaline environment facilitated the in situ formation of Mg/Al LDH, which primarily sequestrated Se(VI) in the interlayer space rather than the Cl^- ions through outer-sphere complexation, consequently precipitating as a sludge. The Se(VI)-sequestration pathway by this method is illustrated in Fig. 5i.

3.6. Reusability of the generated layered double hydroxide sludge

Considering sustainability and practical applicability, we explored the reusability of the generated sludges instead of their disposal as waste. Therefore, the cured sludge for generating crystalline LDH (LDHS) and its calcined sample (LDOS) were examined as Se(VI) adsorbents. XRD analysis of both adsorbents (Fig. 6b) showed that LDHS exhibited a more crystalline LDH phase, characterized by stronger (003) and (006) peaks, compared to uncured samples (Fig. 1e and 2e). A well-crystalline LDH is required as an adsorbent, as the low-crystalline form readily dissolves in aqueous systems. (Goh et al., 2010). Thus, these results represented the applicability of LDHS as an adsorbent. Conversely, the peaks reflecting the LDH phase, i.e., the (003) and (006) planes, disappeared from the calcination process. The disappearance was ascribed to the loss of interlayer anions along with water molecules under high-temperature conditions, resulting in the collapse of the LDH interlayer and its transformation into layered double oxide (LDO) (Lee et al., 2018b). This XRD result correlated with the SEM images of LDHS and LDOS (Fig. 6a and d).

The adsorption characteristics of LDHS and LDOS were investigated as functions of time and the Se(VI) concentrations. The data were fitted to kinetics and isotherm models, with results shown in Fig. 6c and f, and Tables S2 and S3. The LDHS attained faster reaction equilibrium compared to the slower reaction with LDOS, whereas LDOS exhibited higher adsorption capacity. The maximum adsorption capacity of LDOS

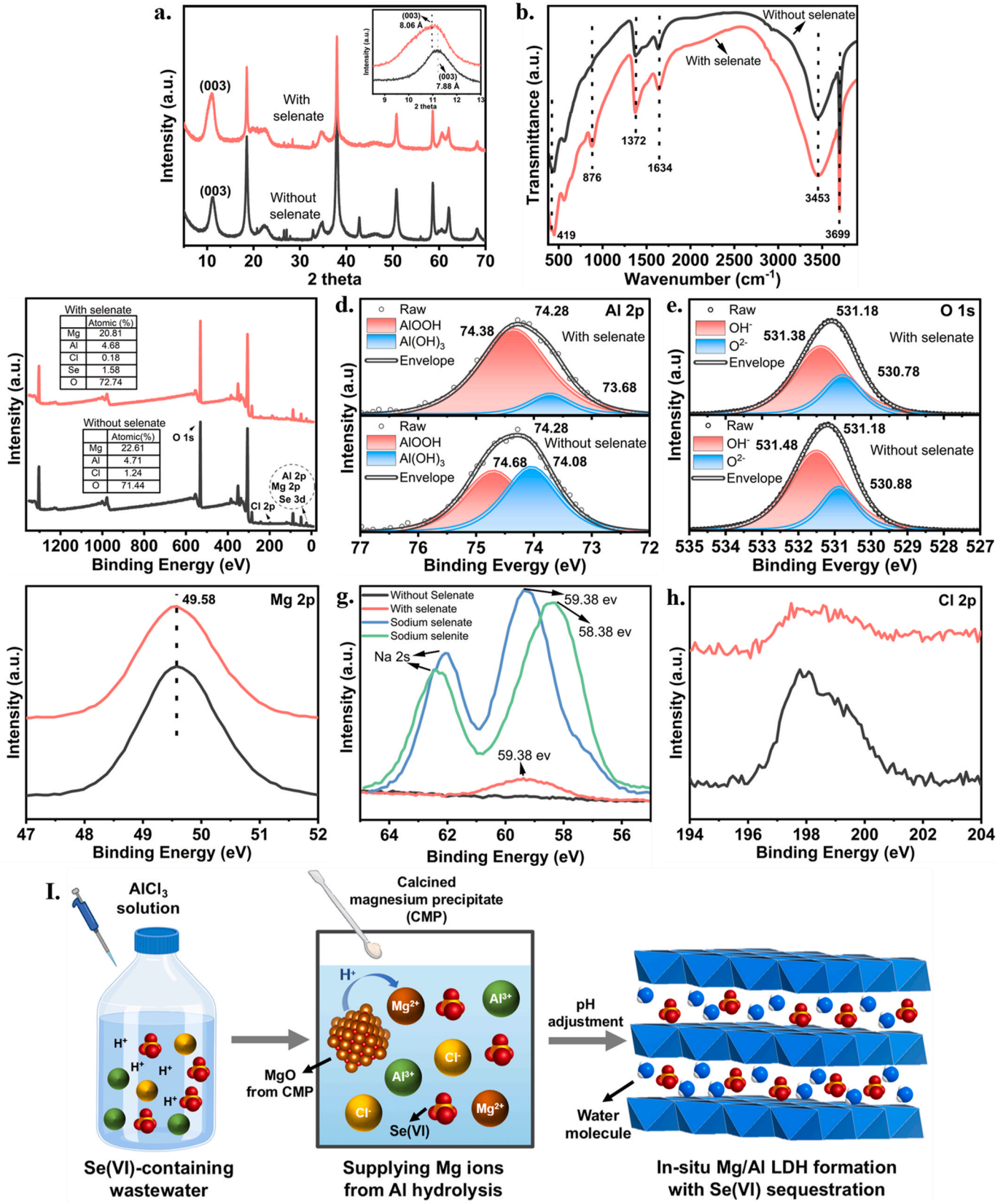

With selenate	Atomic (%)
Mg	20.81
Al	4.68
Cl	0.18
Se	1.58
O	72.74

Without selenate	Atomic(%)
Mg	22.61
Al	4.71
Cl	1.24
O	71.44

Fig. 5. (a) XRD patterns and (b) FTIR spectra of the in situ–formed LDH sludge in the presence (with) and absence (without) of Se(VI). (c) XPS full and narrow spectra of the (d) Al 2p, (e) O 1s, (f) Mg 2p, (g) Se 3d, and (h) Cl 2p peaks of the in situ–formed LDH sludges in the presence (with) and absence (without) of Se(VI). (I) Schematic illustration of the Se(VI) sequestration pathway via in situ LDH formation using CMP and Al hydrolysis.

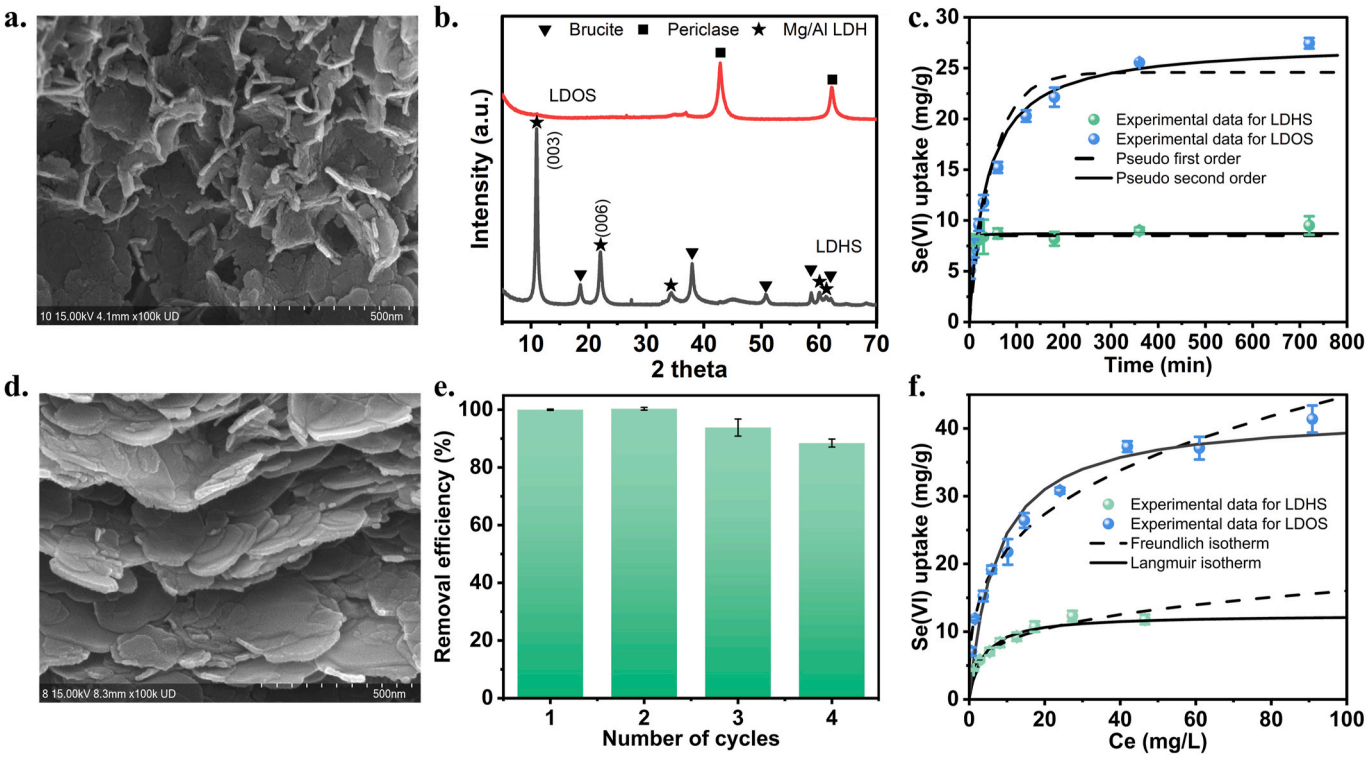

Fig. 6. SEM images of (a) precipitated sludges (LDHS) and (d) calcined precipitated sludges (LODS). (b) XRD patterns of LDHS and CLDHS including brucite (PDF No. 96-100-0055), Mg/Al LDH (hydrotalcite) (PDF No. 96-900-9273), and periclase (PDF No. 96-900-6786). (e) Recycling performance of CLDHS and (c) adsorption kinetics and (f) isotherms of LDHS and LDOS; (C_0: 20 mg/L for kinetics and recycling experiments and 0–100 mg/L for isotherm experiments, absorbent dosage: 0.25 g/L, pH: 7.00 ± 0.05, temperature: 25 °C, ionic strength: 10 mM, and reaction time: 12 h).

(42.1 mg/g), as calculated by the Langmuir model, was much higher than that of LDHS (12.8 mg/g). As aforementioned, LDO contains fewer anions due to the loss of interlayer anions. In aqueous phases, LDO can reconstruct the LDH phase through a memory effect and intercalate surrounding anions (Lee et al., 2018a; Yang et al., 2005). Additionally, LDO generally exhibits a higher surface area than uncalcined LDH due to structural transformation caused by the decomposition of LDH into layered double oxide (LDO) (Fig. 6a and d), resulting in different removal efficiencies (Lee et al., 2018b; Tran et al., 2019; Yang et al., 2005). Therefore, we recommend applying the calcination process for reusing the generated sludge, rather than employing solely LDHS. Compared with the Se(VI) removal efficiency of the in situ LDH formation (127 mg/g in Fig. S5), that of LDOS was low. However, under the experimental pH condition, the efficiency of LDOS was very compatible with that of reported LDHs or other Se(VI) adsorbents (Table 1). Moreover, the sorption efficiency of LDOS was maintained at >88% in its 4th cycle (Fig. 6e) compared with that of fresh LDOS, indicating its applicability as an adsorbent and the sustainability of this green Se(VI) removal method.

3.7. Environmental implications

Se(VI) is more challenging to remove than Se(IV) (Liang et al., 2015; Mondal et al., 2004; Tang et al., 2016), but LDH has proven effective for its removal (Chubar, 2014; Chubar and Szlachta, 2015). Recent studies on LDH adsorption have emphasized practical considerations, such as energy efficiency, cost-effectiveness, and environmental sustainability (Feng et al., 2022), rather than the conventional adsorption process after its laboratory-scale ex-situ synthesis (Fig. S1). Therefore, we focused on using CMP, a waste material with very high Mg content, as a precursor for in situ Mg/Al LDH to remove Se(VI). This method offers a simpler alternative (Fig. S2) compared to the conventional ex-situ LDH preparation followed by Se(VI) adsorption, suggesting further economic advantages. Moreover, no strong acids, such as HNO_3, were utilized for Mg extraction from CMP, providing environmental advantages. The applicability of the generated sludge further highlighted its potential environmental benefits. This study provided insights into sustainable Se (VI) removal by in situ LDH formation from Mg-containing waste (CMP). We believe that this novel and green method can be extended to other solid wastes and natural ores containing Me^{2+} (e.g., Mg^{2+}, Ca^{2+}, and Fe^{2+}) for the removal of hazardous anionic pollutants.

4. Conclusion

This study aimed to sequester Se(VI) through in situ Mg/Al LDH formation via Al hydrolysis, utilizing calcined magnesium precipitate (CMP) as a green precursor. Kinetic experiments optimized the solution pH and Al dosage for Se(VI) removal. Under optimal conditions (Mg/Al molar ratio of 5 and pH 10), a high Se(VI) removal efficiency of 127 mg/g-CMP was achieved with low residual Al. The highest removal efficiency (98.8%) was obtained in a 20 mg/L Se(VI) solution under optimal conditions with increased CMP dosage. Therefore, this method could be suitable for Se(VI) removal in solutions contaminated with high Se(VI) concentrations. The removal efficiency was stable in the presence of humic acid and monovalent ions but decreased with increasing ionic strengths. XRD and FTIR analyses of the precipitated sludge confirmed the intercalation of Se(VI), and the XPS analysis indicated the indirect interaction between Se(VI) and the LDH surface. The overall results suggest that Mg ions are initially released from CMP via Al hydrolysis. Subsequently, Se(VI) is intercalated through outer-sphere complexation within the interlayer of Mg/Al LDH sheets, facilitated by pH adjustment. Furthermore, the precipitated sludge after the reaction was cured (LDHS) and calcined (LDOS) to produce sustainable adsorbents. LDHS and LDOS exhibited adsorption capacities of 12.8 and 42.1 mg/g, respectively, which are comparable to those of reported LDHs and other adsorbents. This study demonstrated a practical in situ LDH formation

method utilizing a sustainable Mg-based precursor for Se(VI) sequestration. This novel approach could be applied in the future to remove other hazardous anionic pollutants from various solid wastes.

CRediT authorship contribution statement

Han Gyeol Jeon: Writing – original draft, Methodology, Investigation, Formal analysis, Data curation, Conceptualization. **Jin-Seok Kim:** Writing – review & editing, Methodology, Data curation. **Seonggyu Choi:** Writing – review & editing, Methodology, Data curation. **Kyung-Hee Lee:** Writing – review & editing, Validation, Data curation, Conceptualization. **Kyoung-Woong Kim:** Writing – review & editing, Validation, Supervision, Methodology, Formal analysis. **Sang-Ho Lee:** Writing – review & editing, Validation, Supervision, Methodology, Investigation, Formal analysis, Conceptualization.

Declaration of competing interest

The authors declare that they have no known competing financial interests or personal relationships that could have appeared to influence the work reported in this paper.

Acknowledgement

This work was supported by the Institute for Korea Spent Nuclear Fuel (iKSNF) and National Research Foundation of Korea (NRF) grant funded by the Korea government (Ministry of Science and ICT, MSIT) (No. 2021M2E1A1085202 and 2021R1A2C1094272).

Appendix A. Supplementary data

Supplementary data to this article can be found online at https://doi.org/10.1016/j.jenvman.2025.125130.

Data availability

The data that has been used is confidential.

References

Basumallick, S., Santra, S., 2017. Monitoring of ppm level humic acid in surface water using ZnO–chitosan nano-composite as fluorescence probe. Appl. Water Sci. 7, 1025–1031. https://doi.org/10.1007/s13201-015-0291-1.

Bernard, E., Zucha, W.J., Lothenbach, B., Mäder, U., 2022. Stability of hydrotalcite (Mg-Al layered double hydroxide) in presence of different anions. Cem Concr Res 152. https://doi.org/10.1016/j.cemconres.2021.106674.

Boclair, J.W., Braterman, P.S., 1999. Layered double hydroxide stability. 1. Relative stabilities of layered double hydroxides and their simple counterparts. Chem. Mater. 11, 298–302. https://doi.org/10.1021/cm980523u.

Cavani, F., Trifirb, F., Vaccari, A., 1991. Hydrotalcite-type anionic clays: preparation, properties and applications. Catal. Today 11, 173–301. https://doi.org/10.1016/0920-5861(91)80068-K.

Chan, Y.T., Liu, Y.T., Tzou, Y.M., Kuan, W.H., Chang, R.R., Wang, M.K., 2018. Kinetics and equilibrium adsorption study of selenium oxyanions onto Al/Si and Fe/Si coprecipitates. Chemosphere 198, 59–67. https://doi.org/10.1016/j.chemosphere.2018.01.110.

Chao, H.P., Wang, Y.C., Tran, H.N., 2018. Removal of hexavalent chromium from groundwater by Mg/Al-layered double hydroxides using characteristics of in-situ synthesis. Environ. Pollut. 243, 620–629. https://doi.org/10.1016/j.envpol.2018.08.033.

Chen, Z., Huang, Z., Liu, J., Wu, E., Zheng, Q., Cui, L., 2021. Phase transition of Mg/Al-flocs to Mg/Al-layered double hydroxides during flocculation and polystyrene nanoplastics removal. J. Hazard Mater. 406. https://doi.org/10.1016/j.jhazmat.2020.124697.

Chinthala, M., Balakrishnan, A., Venkataraman, P., Manaswini Gowtham, V., Polagani, R.K., 2021. Synthesis and applications of nano-MgO and composites for medicine, energy, and environmental remediation: a review. Environ. Chem. Lett. https://doi.org/10.1007/s10311-021-01299-4.

Chubar, N., 2014. EXAFS and FTIR studies of selenite and selenate sorption by alkoxide-free sol-gel generated Mg-Al-CO3layered double hydroxide with very labile interlayer anions. J Mater Chem A Mater 2, 15995–16007. https://doi.org/10.1039/c4ta03463e.

Chubar, N., 2018. The influence of sulfate on selenate sorption on Mg-Al-CO 3 layered double hydroxides prepared by fine inorganic sol-gel synthesis studied by X-ray photoelectron spectroscopy. Appl. Surf. Sci. 459, 281–291. https://doi.org/10.1016/j.apsusc.2018.07.193.

Chubar, N., Szlachta, M., 2015. Static and dynamic adsorptive removal of selenite and selenate by alkoxide-free sol-gel-generated Mg-Al-CO3 layered double hydroxide: effect of competing ions. Chem. Eng. J. 279, 885–896. https://doi.org/10.1016/j.cej.2015.05.070.

Constantino, L.V., Quirino, J.N., Monteiro, A.M., Abrão, T., Parreira, P.S., Urbano, A., Santos, M.J., 2017. Sorption-desorption of selenite and selenate on Mg-Al layered double hydroxide in competition with nitrate, sulfate and phosphate. Chemosphere 181, 627–634. https://doi.org/10.1016/j.chemosphere.2017.04.071.

Cui, W., Li, P., Wang, Z., Zheng, S., Zhang, Y., 2018. Adsorption study of selenium ions from aqueous solutions using MgO nanosheets synthesized by ultrasonic method. J. Hazard Mater. 341, 268–276. https://doi.org/10.1016/j.jhazmat.2017.07.073.

Cullity, B.D., 1956. Elements of X-Ray Diffraction. Addison-Wesley Publishing.

Custelcean, R., Moyer, B.A., 2007. Anion separation with metal-organic frameworks. Eur. J. Inorg. Chem. https://doi.org/10.1002/ejic.200700018.

Das, J., Patra, B.S., Baliarsingh, N., Parida, K.M., 2006. Adsorption of phosphate by layered double hydroxides in aqueous solutions. Appl. Clay Sci. 32, 252–260. https://doi.org/10.1016/j.clay.2006.02.005.

Devi, P., Saroha, A.K., 2017. Utilization of sludge based adsorbents for the removal of various pollutants: a review. Sci. Total Environ. 578, 16–33. https://doi.org/10.1016/j.scitotenv.2016.10.220.

Duan, Z., Li, X., Deng, B.O., 2022. Recent development in the environmental application of nano-sized MgO. Bull. Mater. Sci. 45. https://doi.org/10.1007/s12034-022-02767-5S.

Feng, X., Long, R., Wang, L., Liu, C., Bai, Z., Liu, X., 2022. A Review on Heavy Metal Ions Adsorption from Water by Layered Double Hydroxide and its Composites. Sep Purif Technol. https://doi.org/10.1016/j.seppur.2021.120099.

Forano, C., Hibino, T., Leroux, F., Taviot-Guého, C., 2006. Layered Double Hydroxides, Developments in Clay Science. Elsevier.

Frechou, C., Aguerre, S., Degros, J.P., Kerlau, G., Grangeon, T., 2007. Improvement of a radiochemical separation for selenium 79: applications to effluents and nuclear wastes. Talanta 72, 1166–1171. https://doi.org/10.1016/j.talanta.2007.01.011.

Fruhwirth, O., Herzog, G.W., Hollerer, I., Rachetti, A., 1985. Dissolution and hydration kinetics of MgO. Surf. Technol. 24, 301–317.

Gao, C., Yu, X.Y., Luo, T., Jia, Y., Sun, B., Liu, J.H., Huang, X.J., 2014. Millimeter-sized Mg-Al-LDH nanoflake impregnated magnetic alginate beads (LDH-n-MABs): a novel bio-based sorbent for the removal of fluoride in water. J Mater Chem A Mater 2, 2119–2128. https://doi.org/10.1039/c3ta13526h.

Goh, K.H., Lim, T.T., 2004. Geochemistry of inorganic arsenic and selenium in a tropical soil: effect of reaction time, pH, and competitive anions on arsenic and selenium adsorption. Chemosphere 55, 849–859. https://doi.org/10.1016/j.chemosphere.2003.11.041.

Goh, K.H., Lim, T.T., 2010. Influences of co-existing species on the sorption of toxic oxyanions from aqueous solution by nanocrystalline Mg/Al layered double hydroxide. J. Hazard Mater. 180, 401–408. https://doi.org/10.1016/j.jhazmat.2010.04.045.

Goh, K.H., Lim, T.T., Dong, Z., 2008. Application of layered double hydroxides for removal of oxyanions: a review. Water Res. 42, 1343–1368. https://doi.org/10.1016/j.watres.2007.10.043.

Goh, K.H., Lim, T.T., Banas, A., Dong, Z., 2010. Sorption characteristics and mechanisms of oxyanions and oxyhalides having different molecular properties on Mg/Al layered double hydroxide nanoparticles. J. Hazard Mater. 179, 818–827. https://doi.org/10.1016/j.jhazmat.2010.03.077.

Gonzalez, C.M., Hernandez, J., Parsons, J.G., Gardea-Torresdey, J.L., 2010. A study of the removal of selenite and selenate from aqueous solutions using a magnetic iron/manganese oxide nanomaterial and ICP-MS. Microchem. J. 96, 324–329. https://doi.org/10.1016/j.microc.2010.05.005.

Goswamee, R.L., Sengupta, P., Gopal Bhattacharyya, K., Dutta, K., 1998. Adsorption of Cr (VI) in layered double hydroxides. Appl. Clay Sci. 13, 21–34. https://doi.org/10.1016/S0169-1317(98)00010-6.

Gu, C., Wang, Z., Kubicki, J.D., Wang, X., Zhu, M., 2016. X-Ray absorption spectroscopic quantification and speciation modeling of sulfate adsorption on ferrihydrite surfaces. Environ. Sci. Technol. 50, 8067–8076. https://doi.org/10.1021/acs.est.6b00753.

Guo, B., Sasaki, K., Hirajima, T., 2017. Selenite and selenate uptaken in ettringite: immobilization mechanisms, coordination chemistry, and insights from structure. Cem Concr Res 100, 166–175. https://doi.org/10.1016/j.cemconres.2017.07.004.

Han, S., Hou, W., Zhang, C., Sun, D., Huang, X., Wang, G., 1998. Structure and the point of zero charge of magnesium aluminium hydroxide. J. Chem. Soc., Faraday Trans. 94, 915–918.

Hong, S.H., Lyonga, F.N., Kang, J.K., Seo, E.J., Lee, C.G., Jeong, S., Hong, S.G., Park, S.J., 2020. Synthesis of Fe-impregnated biochar from food waste for Selenium(VI) removal from aqueous solution through adsorption: process optimization and assessment. Chemosphere 252. https://doi.org/10.1016/j.chemosphere.2020.126475.

Huang, Zhiyan, Wang, T., Shen, M., Huang, Zhujian, Chong, Y., Cui, L., 2019. Coagulation treatment of swine wastewater by the method of in-situ forming layered double hydroxides and sludge recycling for preparation of biochar composite catalyst. Chem. Eng. J. 369, 784–792. https://doi.org/10.1016/j.cej.2019.03.136.

Ivanets, A., Prozorovich, V., Roshchina, M., Kouznetsova, T., Budeiko, N., Kulbitskaya, L., Hosseini-Bandegharaei, A., Masindi, V., Pankov, V., 2021. A comparative study on the synthesis of magnesium ferrite for the adsorption of metal ions: insights into the essential role of crystallite size and surface hydroxyl groups. Chem. Eng. J. 411. https://doi.org/10.1016/j.cej.2021.128523.

Jeon, H.G., Choi, S., Kim, J.-S., Lee, K.-H., Shin, J., Chon, K., Kim, K.-W., Lee, S.-H., 2024. Mechanistic Insights into selenite and selenate immobilization using brucite-rich

magnesium precipitate derived from seawater electrochlorination facility. J. Environ. Chem. Eng. 12, 114081. https://doi.org/10.1016/j.jece.2024.114081.
Ji, H., Wu, W., Li, F., Yu, X., Fu, J., Jia, L., 2017. Enhanced adsorption of bromate from aqueous solutions on ordered mesoporous Mg-Al layered double hydroxides (LDHs). J. Hazard Mater. 334, 212–222. https://doi.org/10.1016/j.jhazmat.2017.04.014.
Jiang, Z., Wu, J., Liu, X., Yu, H., Jiao, C., Shen, J., Pei, Y., 2021. Facile synthesis of MgAl layered double hydroxides by a co-precipitation method for efficient nitrate removal from water: kinetics and mechanisms. New J. Chem. 45, 14580–14588. https://doi.org/10.1039/d1nj02035h.
Jiang, Y., Shen, Z., Tang, C.S., Shi, B., 2023. Synthesis and application of waste-based layered double hydroxide: a review. Sci. Total Environ. 903. https://doi.org/10.1016/j.scitotenv.2023.166245.
Jing, F., Zhang, Y., Luo, S., Chu, W., Qian, W., 2010. Nano-size MZnAl (M = Cu, Co, Ni) metal oxides obtained by combining hydrothermal synthesis with urea homogeneous precipitation procedures. Appl. Clay Sci. 48, 203–207. https://doi.org/10.1016/j.clay.2009.11.039.
Jordan, N., Franzen, C., Lützenkirchen, J., Foerstendorf, H., Hering, D., Weiss, S., Heim, K., Brendler, V., 2018. Adsorption of selenium(VI) onto nano transition alumina. Environ. Sci. Nano 5, 1661–1669. https://doi.org/10.1039/c8en00293b.
Kuwahara, Y., Yamashita, H., 2013. A new catalytic opportunity for waste materials: application of waste slag based catalyst in CO2 fixation reaction. J. CO2 Util. 1, 50–59. https://doi.org/10.1016/j.jcou.2013.03.001.
Lee, S.H., Takahashi, Y., 2019. Carbothermal preparation of magnetic-responsible ferrihydrite based on Fe-rich precipitates for immobilization of arsenate and antimonate: batch and spectroscopic studies. Chemosphere 237. https://doi.org/10.1016/j.chemosphere.2019.124489.
Lee, S.H., Choi, H., Kim, K.W., 2018a. Removal of As(V) and Sb(V) in aqueous solution by Mg/Al-layered double hydroxide-incorporated polyethersulfone polymer beads (PES-LDH). Environ. Geochem. Health 40, 2119–2129. https://doi.org/10.1007/s10653-018-0087-y.
Lee, S.H., Tanaka, M., Takahashi, Y., Kim, K.W., 2018b. Enhanced adsorption of arsenate and antimonate by calcined Mg/Al layered double hydroxide: Investigation of comparative adsorption mechanism by surface characterization. Chemosphere 211, 903–911. https://doi.org/10.1016/j.chemosphere.2018.07.153.
Lee, K.H., Lee, Y.G., Shin, J., Chon, K., Lee, S.H., 2020. Selective immobilization of antimony using brucite-rich precipitate produced during in situ hypochlorous acid formation through seawater electrolysis in a nuclear power plant. Energies 13. https://doi.org/10.3390/en13174493.
Lee, N., Hong, S.H., Lee, C.G., Park, S.J., Lee, J., 2021. Conversion of cattle manure into functional material to remove selenate from wastewater. Chemosphere 278. https://doi.org/10.1016/j.chemosphere.2021.130398.
Letavayová, L., Vlčková, V., Brozmanová, J., 2006. Selenium: from cancer prevention to DNA damage. Toxicology 227, 1–14. https://doi.org/10.1016/j.tox.2006.07.017.
Liang, L., Yang, W., Guan, X., Li, J., Xu, Z., Wu, J., Huang, Y., Zhang, X., 2013. Kinetics and mechanisms of pH-dependent selenite removal by zero valent iron. Water Res. 47, 5846–5855. https://doi.org/10.1016/j.watres.2013.07.011.
Liang, L., Guan, X., Huang, Y., Ma, J., Sun, X., Qiao, J., Zhou, G., 2015. Efficient selenate removal by zero-valent iron in the presence of weak magnetic field. Sep. Purif. Technol. 156, 1064–1072. https://doi.org/10.1016/j.seppur.2015.09.062.
Lounsbury, A.W., Yamani, J.S., Johnston, C.P., Larese-Casanova, P., Zimmerman, J.B., 2016. The role of counter ions in nano-hematite synthesis: implications for surface area and selenium adsorption capacity. J. Hazard Mater. 310, 117–124. https://doi.org/10.1016/j.jhazmat.2016.01.078.
Mccusker, L.B., Von Dreele, R.B., Cox, D.E., Loue, D., Scardi, P., 1999. Rietveld refinement guidelines. International Union of Crystallography Journal of Applied Crystallography J. Appl. Cryst 32, 36–50.
Min, L., Duan, J., Liu, L., Ge, S., Zhang, W., Wang, Y., 2022. Efficient, scalable, closed-loop synthesis of highly crystalline pure phase MgAl-layered double hydroxides intercalated with hydroxyl anions. Dalton Trans. 51, 2033–2040. https://doi.org/10.1039/d1dt03849d.
Mondal, K., Jegadeesan, G., Lalvani, S.B., 2004. Removal of selenate by Fe and NiFe nanosized particles. Ind. Eng. Chem. Res. 43, 4922–4934. https://doi.org/10.1021/ie030715l.
Muriithi, G.N., Petrik, L.F., Gitari, W.M., Doucet, F.J., 2017. Synthesis and characterization of hydrotalcite from South African Coal fly ash. Powder Technol. 312, 299–309. https://doi.org/10.1016/j.powtec.2017.02.018.
Paikaray, S., Hendry, M.J., Essilfie-Dughan, J., 2013. Controls on arsenate, molybdate, and selenate uptake by hydrotalcite-like layered double hydroxides. Chem. Geol. 345, 130–138. https://doi.org/10.1016/j.chemgeo.2013.02.015.
Palmer, S.J., Frost, R.L., Nguyen, T., 2009. Hydrotalcites and their role in coordination of anions in Bayer liquors: anion binding in layered double hydroxides. Coord. Chem. Rev. 253, 250–267. https://doi.org/10.1016/j.ccr.2008.01.012.
Peak, D., 2006. Adsorption mechanisms of selenium oxyanions at the aluminum oxide/water interface. J. Colloid Interface Sci. 303, 337–345. https://doi.org/10.1016/j.jcis.2006.08.014.
Phanthasri, J., Yan, D.Y.S., Wantala, K., Khunphonoi, R., Khamdahsag, P., Tanboonchuy, V., 2023. Selenate removal via continuous fixed-bed column with nanoscale zero-valent iron supported on bentonite-zeolite pellets. J. Water Proc. Eng. 53. https://doi.org/10.1016/j.jwpe.2023.103843.
Pokrovsky, O.S., Schott, J., Castillo, A., 2005. Kinetics of brucite dissolution at 25°C in the presence of organic and inorganic ligands and divalent metals. Geochim Cosmochim Acta 69, 905–918. https://doi.org/10.1016/j.gca.2004.08.011.
Qiu, X., Sasaki, K., Hirajima, T., Ideta, K., Miyawaki, J., 2013. Temperature effect on the sorption of borate by a layered double hydroxide prepared using dolomite as a magnesium source. Chem. Eng. J. 225, 664–672. https://doi.org/10.1016/j.cej.2013.03.099.
Ren, J., Leus, K., Morent, R., De Geyter, N., Van Der Voort, P., Du Laing, G., 2024. Fe(III)-alginate and layered aluminum oxyhydroxide assisted hydro ceramsite composite for efficient removal of Se and as from high-concentration sulfate wastewater. Sep. Purif. Technol. 334. https://doi.org/10.1016/j.seppur.2023.126101.
Rodríguez-Carvajal, J., 2021. An Introduction to the Program: FullProf 2000 (Version July 2001).
Ruj, B., Bishayee, B., Chatterjee, R.P., Mukherjee, A., Saha, A., Nayak, J., Chakrabortty, S., 2022. An economical strategy towards the managing of selenium pollution from contaminated water: a current state-of-the-art review. J. Environ. Manag. 304. https://doi.org/10.1016/j.jenvman.2021.114143.
Rybka, K., Matusik, J., Marzec, M., 2022. Mg/Al and Mg/Fe layered double hydroxides derived from magnesite and chemicals: the effect of adsorbent features and anions chemistry on their removal efficiency. J. Clean. Prod. 332. https://doi.org/10.1016/j.jclepro.2021.130084.
Saha, S., Ray, S., Acharya, R., Chatterjee, T.K., Chakraborty, J., 2017. Magnesium, zinc and calcium aluminium layered double hydroxide-drug nanohybrids: a comprehensive study. Appl. Clay Sci. https://doi.org/10.1016/j.clay.2016.09.030.
Santos, S., Ungureanu, G., Boaventura, R., Botelho, C., 2015. Selenium contaminated waters: an overview of analytical methods, treatment options and recent advances in sorption methods. Sci. Total Environ. https://doi.org/10.1016/j.scitotenv.2015.03.107.
Sato, T., Kato, K., Yoshioka, T., Okuwaki, A., 1992. Uptake of benzenecarboxylate ions by magnesium aluminium oxides. J. Chem. Technol. Biotechnol. 55, 385–390. https://doi.org/10.1002/jctb.280550414.
Schofield, R.K., Taylor, A.W., 1954. The hydrolysis of aluminum salt solutions. J. Chem. Soc. 4445–4448.
Shao, S., Zheng, B., 2008. The biogeochemistry of selenium in Sunan grassland, Gansu, Northwest China, casts doubt on the belief that Marco Polo reported selenosis for the first time in history. Environ. Geochem. Health 30, 307–314. https://doi.org/10.1007/s10653-008-9166-9.
Sharmasarkar, S., Vance, G.F., 2002. Selenite selenate sorption in surface coal mine environment. Adv. Environ. Res. 7, 8795. https://doi.org/10.1016/S1093-0191(01)00110-1.
Stefaniak, J., Dutta, A., Verbinnen, B., Shakya, M., Rene, E.R., 2018. Selenium removal from mining and process wastewater: a systematic review of available technologies. J. Water Supply Res. Technol. - Aqua 67, 903–918. https://doi.org/10.2166/aqua.2018.109.
Su C Suarez, D.L., 2000. Selenate and selenite sorption on iron oxides: an infrared and electrophoretic study. Soil Sci. Soc. Am. J. 64, 101–111. https://doi.org/10.2136/sssaj2000.641101x.
Su, C., Suarez, D.L, 2021. Direct electrochemical pathways for selenium reduction in aqueous solutions. ACS Sustain. Chem. Eng. 9, 2027–2036. https://doi.org/10.1021/acssuschemeng.0c06585.
Sun, W., Pan, W., Wang, F., Xu, N., 2015. Removal of Se(IV) and Se(VI) by MFe2O4 nanoparticles from aqueous solution. Chem. Eng. J. 273, 353–362. https://doi.org/10.1016/j.cej.2015.03.061.
Sun, W., Renew, J.E., Zhang, W., Tang, Y., Huang, C.H., 2017. Sorption of Se(IV) and Se (VI) to coal fly ash/cement composite: effect of Ca2 + and high ionic strength. Chem. Geol. 464, 76–83. https://doi.org/10.1016/j.chemgeo.2016.12.041.
Tang, C., Huang, Y., Zhang, Z., Chen, J., Zeng, H., Huang, Y.H., 2016. Rapid removal of selenate in a zero-valent iron/Fe3O4/Fe2+ synergetic system. Appl. Catal., B 184, 320–327. https://doi.org/10.1016/j.apcatb.2015.11.045.
Theiss, F.L., Couperthwaite, S.J., Ayoko, G.A., Frost, R.L., 2014. A review of the removal of anions and oxyanions of the halogen elements from aqueous solution by layered double hydroxides. J. Colloid Interface Sci. 417, 356–368. https://doi.org/10.1016/j.jcis.2013.11.040.
Theiss, F.L., Ayoko, G.A., Frost, R.L., 2016. Synthesis of layered double hydroxides containing Mg 2+ , Zn 2+ , Ca 2+ and Al 3+ layer cations by co-precipitation methods - a review. Appl. Surf. Sci. 383, 200–213. https://doi.org/10.1016/j.apsusc.2016.04.150.
Tian, Q., Guo, B., Sasaki, K., 2020. Influence of silicate on the structural memory effect of layered double hydroxides for the immobilization of selenium. J. Hazard Mater. 395. https://doi.org/10.1016/j.jhazmat.2020.122674.
Tran, H.N., Nguyen, D.T., Le, G.T., Tomul, F., Lima, E.C., Woo, S.H., Sarmah, A.K., Nguyen, H.Q., Nguyen, P.T., Nguyen, D.D., Nguyen, T.V., Vigneswaran, S., Vo, D.V. N., Chao, H.P., 2019. Adsorption mechanism of hexavalent chromium onto layered double hydroxides-based adsorbents: a systematic in-depth review. J. Hazard Mater. 373, 258–270. https://doi.org/10.1016/j.jhazmat.2019.03.018.
Tsuchiya, K., Fuchida, S., Tokoro, C., 2023. Synthesis and selenate removal of magnesium–aluminum-layered double hydroxide particle using magnesium oxide. Int. J. Environ. Sci. Technol. 20, 9481–9494. https://doi.org/10.1007/s13762-022-04653-3.
Ullah, H., Liu, G., Yousaf, B., Ali, M.U., Irshad, S., Abbas, Q., Ahmad, R., 2019. A comprehensive review on environmental transformation of selenium: recent advances and research perspectives. Environ. Geochem. Health 41, 1003–1035. https://doi.org/10.1007/s10653-018-0195-8.
Ullah, H., Lun, L., Rashid, A., Zada, N., Chen, B., Shahab, A., Li, P., Ali, M.U., Lin, S., Wong, M.H., 2023. A critical analysis of sources, pollution, and remediation of selenium, an emerging contaminant. Environ. Geochem. Health 45, 1359–1389. https://doi.org/10.1007/s10653-022-01354-1.
USEPA, 2017. Secondary Drinking Water Standards: Guidance for Nuisance Chemicals.
USEPA, 2024. National Primary Drinking Water Regulations. Washington, DC, USA.
Wang, X., Li, W., Harrington, R., Liu, F., Parise, J.B., Feng, X., Sparks, D.L., 2013. Effect of ferrihydrite crystallite size on phosphate adsorption reactivity. Environ. Sci. Technol. 47, 10322–10331. https://doi.org/10.1021/es401301z.

Wang, Q., Lin, Q., Li, Q., Li, K., Wu, L., Li, S., Liu, H., 2021. As(III) removal from wastewater and direct stabilization by in-situ formation of Zn-Fe layered double hydroxides. J. Hazard Mater. 403. https://doi.org/10.1016/j.jhazmat.2020.123920.

Wu, L., Pan, F., Liu, Y., Zhang, G., Tang, A., Atrens, A., 2018. Influence of pH on the growth behaviour of Mg–Al LDH films. Surf. Eng. 34, 674–681. https://doi.org/10.1080/02670844.2017.1382062.

Xi, M., Zhang, C., Ma, H., Zhou, Z., Zhu, K., Jia, H., 2023. Atomic-scale understanding of Se(IV) surface complexation on gibbsite: insights from first-principles molecular dynamics. Chem. Geol. 638. https://doi.org/10.1016/j.chemgeo.2023.121716.

Xu, L., Huang, Y., 2019. A novel layered double hydroxide coupled with zero valent iron system for selenate removal under anaerobic condition: batch and continuous studies. Chem. Eng. J. 359, 1166–1174. https://doi.org/10.1016/j.cej.2018.11.061.

Xu, S., Zhong, Z., Liu, W., Deng, H., Lin, Z., 2020. Removal of Sb(III) from wastewater by magnesium oxide and the related mechanisms. Environ. Res. 186. https://doi.org/10.1016/j.envres.2020.109489.

Yamani, J.S., Lounsbury, A.W., Zimmerman, J.B., 2014. Adsorption of selenite and selenate by nanocrystalline aluminum oxide, neat and impregnated in chitosan beads. Water Res. 50, 373–381. https://doi.org/10.1016/j.watres.2013.10.054.

Yang, L., Shahrivari, Z., Liu, P.K.T., Sahimi, M., Tsotsis, T.T., 2005. Removal of trace levels of arsenic and selenium from aqueous solutions by calcined and uncalcined layered double hydroxides (LDH). Ind. Eng. Chem. Res. 44, 6804–6815. https://doi.org/10.1021/ie049060u.

You, Y., Vance, G.F., Zhao, H., 2001. Selenium adsorption on Mg-Al and Zn-Al layered double hydroxides. Appl. Clay Sci. 20, 13–25. https://doi.org/10.1016/S0169-1317(00)00043-0.

Yue, P., Chen, N., Peak, D., Bompoti, N.M., Chrysochoou, M., Onnis-Hayden, A., Larese-Casanova, P., 2020. Oxygen atom release during selenium oxyanion adsorption on goethite and hematite. Appl. Geochem. 117. https://doi.org/10.1016/j.apgeochem.2020.104605.

Zelmanov, G., Semiat, R., 2013. Selenium removal from water and its recovery using iron (Fe3+) oxide/hydroxide-based nanoparticles sol (NanoFe) as an adsorbent. Sep. Purif. Technol. 103, 167–172. https://doi.org/10.1016/j.seppur.2012.10.037.

Zhao, C.X., Ma, X.P., Duan, X.L., Guo, Q., Niu, S.L., Zhou, W.J., Cao, Y.M., Yuan, C.G., 2023. Synthesis of novel adsorbent S-SiO2@Fe3O4 based on strong bonding of S-O-Se for selenium removal in water. J. Environ. Chem. Eng. 11. https://doi.org/10.1016/j.jece.2023.109782.

Zhou, Y.F., Haynes, R.J., 2012. A comparison of water treatment sludge and red mud as adsorbents of as and Se in aqueous solution and their capacity for desorption and regeneration. Water Air Soil Pollut. 223, 5563–5573. https://doi.org/10.1007/s11270-012-1296-0.

Zhu, J., Zeng, B., Mo, L., Jin, F., Deng, M., Zhang, Q., 2021. One-pot synthesis of Mg [sbnd]Al layered double hydroxide (LDH) using MgO and metakaolin (MK) as precursors. Appl. Clay Sci. 206. https://doi.org/10.1016/j.clay.2021.106070.

Zoroufchi, B.K., Sokhansanj, A., Hughes, K.A., McPhedran, K.N., Soltan, J., 2023. An engineered biochar for treatment of selenite contaminated water: mass transfer characteristics in fixed bed adsorption. Chem. Eng. J. 469. https://doi.org/10.1016/j.cej.2023.143946.